Strategies for mitigating the strong direct path signal in passive bistatic SAR imaging

Virginie Kubica, Edison Cristofani, Xavier Neyt
Royal Military Academy of Belgium, Electrical Engineering Dept.
Avenue de la Renaissance 30, B-1000 Brussels, Belgium

Abstract

For non-cooperative bistatic SAR, one of the major issue is the direct path interference. This signal will also enter the receiver and seriously impact the SAR imaging.

The image synthesis is based on the direct application of the matched filter. Imaging in the immediate surrounding of the receiver will be impaired by the range and azimuth sidelobes of the strong direct path signal caused by the conventional matched-filter-based SAR processing.

In this paper, we present two methods to mitigate the range and azimuth sidelobes of the strong direct path signal: adaptive digital nullsteering and apodization of the matched filter. These methods are first evaluated on simulated signals. Next, field experiments using the European Space Agency's ENVISAT satellite as transmitter of opportunity will validate this processing.

1 Introduction

Unlike monostatic SAR, opportunistic bistatic SAR is affected by the strong direct path signal coming directly from the illuminator of opportunity. After the conventional matched-filter-based SAR processing, this leads to range and azimuth sidelobes that can easily interfere or obscure nearby scatterers which have weaker return signal strength. Sidelobe reduction strategies have to be considered to mitigate the effects of this strong reference signal.

The first considered strategy is the spatial adaptive nullsteering, which attenuates or even eliminates the direct path signal in a similar way as we did in [1]. This adaptive algorithm is all the more powerful since the illuminator of opportunity is moving. This processing also retrieves the reference signal needed to perform the synchronisation in SAR imaging. The considered phased-array antenna is a patch antenna array of four elements. To cope with mutual coupling effects and manufacturing tolerances, array calibration is required [2].

The second strategy to mitigate the strong direct path signal is to apply appropriate weighting functions to the matched filter, a technique known by the general term apodization.

In this paper, we study the performance of these two strategies and the impact on the imaging range in our application of space-surface bistatic SAR.

The paper is organized as follows. Section 2 describes the designed passive bistatic radar. In Section 3, the impacts of the strong direct path signal are presented. Section 4 explains in detail the two attenuation methods while section 5 offers concluding remarks. Finally, we consider future works in Section 6.

2 System overview

The passive bistatic imaging radar consists of an opportunistic spaceborne radar transmitter and a ground-based receiver (Fig. 1).

We use a backscattering geometry, where the receive and the transmit antennas are located on the same side of the illuminated area, to achieve the best possible range resolution [3], [4], [5], [6]. Thanks to this configuration, the direct signal from the satellite will be attenuated since it is received via a sidelobe of the array antenna.

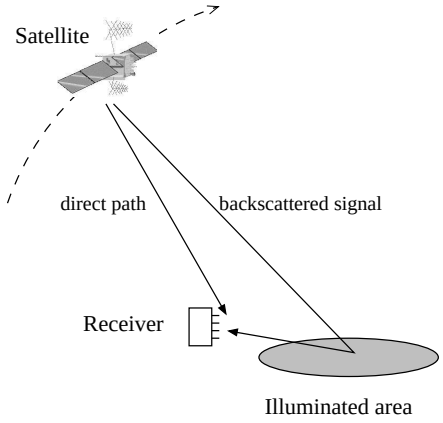

Figure 1: Geometry for bistatic SAR.

3 Effect of the direct path signal

The SAR image synthesis based on the direct application of the matched filter suffers from the masking effect of the range and azimuth sidelobes of the strong direct path signal or of a strong point scatterer. These sidelobes may mask nearby, weaker scatterers or may be mistaken for false echoes. The significant range sidelobes are formed from the rectangular power spectrum of the transmitted chirp giving a sinc shaped correlation function. As for azimuth sidelobes, they are caused by the limited synthetic aperture length and/or by the azimuth radiation pattern of the transmit antenna.

3.1 Range sidelobes

At reception, the transmitted chirp is range-compressed using the matched filter. The impulse response is obtained by compressing the direct path signal of the ENVISAT radar satellite and is a sinc function as represented in Fig 5. The mainlobe and the high levels of the sidelobes hamper imaging along the baseline in the surrounding of the receiver.

3.2 Azimuth sidelobes

To illustrate the azimuth sidelobes due to the SAR processing, we consider a scenario with a point scatterer to the East of the receiver. Figure 2 (a) shows the tangential plane centered at the receiver and the isorange on which the point scatterer is located (300 m from the receiver). After the range compression using the matched-filter, each azimuthal contribution of the signal is coherently integrated along this isorange taking into account the phase history. Figure 2 (b) shows the result which presents two peaks: one corresponding to the position of the point scatterer and one corresponding to its ambiguity, respectively in red and black on Fig. 2 (a). This ambiguity arises out of the two intersections of the line transmitter-target (dashed line on Fig. 2 (a)) with the isorange. This line corresponds to the narrow synthetic beam resulting of the aperture synthesis in azimuth. In practice, since the radiation diagram of the receiving antenna points East, this ambiguity is in the backlobe of the receive antenna and hence does not appear on the SAR image.

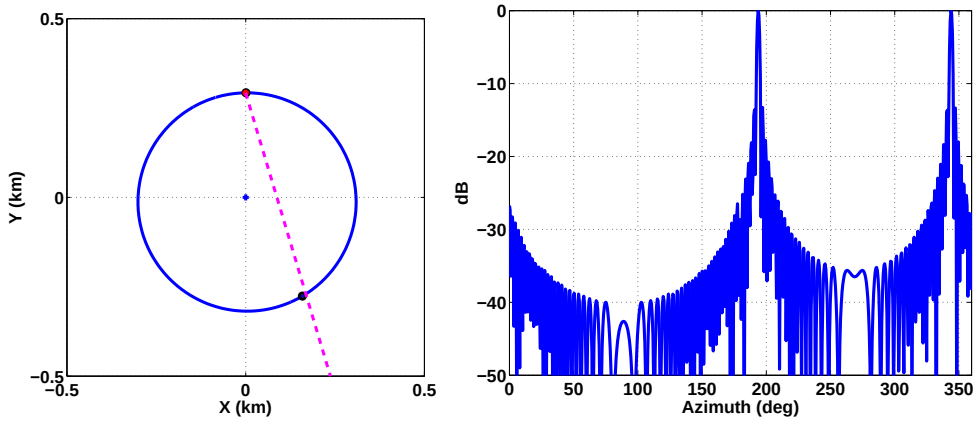

(a) (b)

Figure 2: (a) Scenario with a point scatterer at the East of the receiver and (b) the azimuth sidelobes of a point scatterer.

4 Sidelobe mitigation strategies

To deal with these sidelobes, two strategies have been considered. The first one is the radical method of spatial adaptive nullsteering to attenuate and even suppress the strong direct path signal and thus its sidelobes. The second one is the well-known apodization method which can reduce the sidelobes at the expense of a loss in range and in azimuth resolution.

4.1 Spatial adaptive nullsteering

4.1.1 Spatial filtering

Spatial nullsteering considers here a four-element antenna array to reject the signal coming from the source of opportunity.

We consider the following signal model

$$\mathbf{y} = \alpha \mathbf{s}(\theta) + \beta \mathbf{s}(\theta_i) + \mathbf{n} \tag{1}$$

where $\mathbf{y}$ is the received signal at the antenna array, $\mathbf{s}$ is the array steering vector in the indicated direction θ, α is the complex amplitude of the useful signal, β is the complex amplitude of the interfering signal at the DOA θ_i, $\mathbf{n}$ is the thermal noise. Interference, useful signal and noise are assumed to be uncorrelated. In order to perform that rejection, a matched filter is considered. It is well known [7] that the optimum filter in that case is given by

$$\mathbf{w}(\theta, \theta_i) = \mathbf{R}^{-1}(\mathbf{s}(\theta_i))\mathbf{s}(\theta) \tag{2}$$

where $\mathbf{R}$ is the covariance matrix of the interference + noise and the dependence of the interfering signal on the steering vector is explicitly noted. Considering the simplified model (1), the interference plus noise covariance matrix can be expressed as

$$\mathbf{R}(\mathbf{s}(\theta_i)) = E[|\beta|^2]\mathbf{s}(\theta_i)\mathbf{s}^\dagger(\theta_i) + \sigma^2\mathbf{I} \tag{3}$$

where σ^2 is the variance of the thermal noise and $\mathbf{I}$ is the identity matrix.

A similar filter will be used to extract the direct path signal to perform the synchronisation of the receiver with the transmitter of opportunity which is one of the salient difficulties for non-cooperative bistatic SAR.

4.1.2 Calibration

However, the steering vector for a particular DOA is actually not available. Although suboptimal, a solution consisting in replacing the true steering vectors $\mathbf{s}$ in (2) by estimated steering vectors $\hat{\mathbf{s}}$ yielding

$$\hat{\mathbf{w}} = \hat{\mathbf{R}}^{-1}(\hat{\mathbf{s}}(\theta_i))\hat{\mathbf{s}}(\theta) \tag{4}$$

is a reasonable engineering approach. In [2], two steering vector estimation methods to calibrate an antenna array have been compared using real measurements in an anechoic chamber. The first method is based on a synthesis of the steering vector using a model the parameters which have been estimated using the measured steering vectors. In the second method, the steering vectors are obtained by interpolating between adjacent measured steering vectors. These methods calibrate the array by allowing to estimate the steering vector for a particular θ using a set of measured steering vectors.

The end-to-end performance of the filter $\hat{\mathbf{w}}$ (4), and thus of the steering vector estimation method, have been evaluated by computing the SINR (Signal to Interference plus Noise Ratio) loss [8] defined as

$$\begin{aligned} SINR_{loss}(\theta, \theta_i) &= \frac{SINR_{\text{out}}}{SNR_{in}} \\ &= \frac{|\hat{\mathbf{w}}^{\dagger}(\theta, \theta_i)\mathbf{s}(\theta)|^2}{\hat{\mathbf{w}}^{\dagger}(\theta, \theta_i)\mathbf{R}\hat{\mathbf{w}}(\theta, \theta_i)} \frac{\sigma^2}{\mathbf{s}^{\dagger}(\theta)\mathbf{s}(\theta)}. \end{aligned} \tag{5}$$

The SINR loss can be interpreted as the loss in SINR due to the presence of the interference filtered by the considered filter. The minimal SINR loss is obtained using $\mathbf{w}$ and suboptimal filters $\hat{\mathbf{w}}$ may only further degrade the SINR loss.

We first consider an interference arriving from $\theta_i = 2°$ with a SIR (Signal-to-Interference Ratio) of 0 dB and a SNR (Signal-to Noise Ratio) of 30 dB.

The SINR losses of both methods are illustrated in Fig. 3 as a function of the angle θ. As a comparison, the ideal case for which the filter is calculated using the true measured steering vectors is also shown. As intuitively expected, the performance of the interpolation method decreases as the number of calibration sources diminishes.

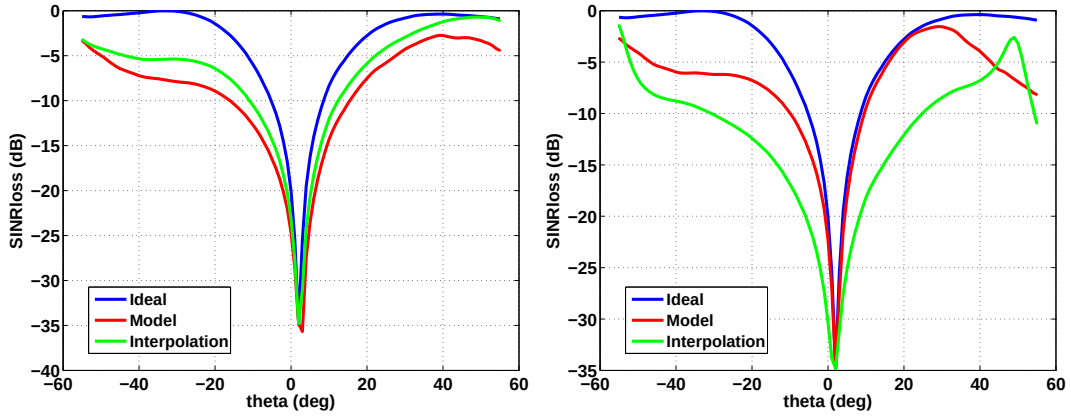

(a) (b)

Figure 3: Comparison of the estimation methods: (a) for 10 calibration sources and (b) for 7 calibration sources

The results suggest that when a large number of steering vectors is available, the interpolation-based method provides better results that the model-based method. The anechoic

chamber calibration procedure has the drawbacks of being time consuming and is not adapted for a changing electromagnetic environment. In the future, the calibration data will be estimated in the field directly from the impinging signals themselves, without the aid of any special calibration source. In addition, in SAR bistatic imaging, measurements at two angles of elevation φ are required: $\varphi_i > 0$ corresponding to the elevation of the interference (illuminator of opportunity) and $\varphi_{obs} < 0$ corresponding to the elevation of the imaged area. The steering vectors at the last elevation angle will be the most difficult to estimate due to the absence of dedicated calibration sources on the ground. This issue could be solved by using the available (point) scatterers in the SAR synthesized image as calibration sources.

4.1.3 Shadowed area

One of the drawbacks of spatial nullsteering is a shadowed area that can appear on the SAR image due to the suppression of the backscattered signals. The considered spatial filter $\mathbf{w}$ (2) will steer a null in a cone angle [9] corresponding to the direction of the transmitter and will affect other directions according to its beampattern. The effect of the beampattern of the spatial filter will be reflected on the SAR image.

To demonstrate this shadowed effect, we consider a scenario in which there are several point scatterers in an area of 2×2 km East of the receiver as depicted in Fig. 4 (a). The optimum beamformer is computed for a look direction θ of -50° and for an interference in the direction θ_i of 0°. In the synthetised image (Fig. 4 (b)), the shape of the beampattern of the spatial filter can be recognized through the amplitudes of the reflections and one can observe the total attenuation of the receiver.

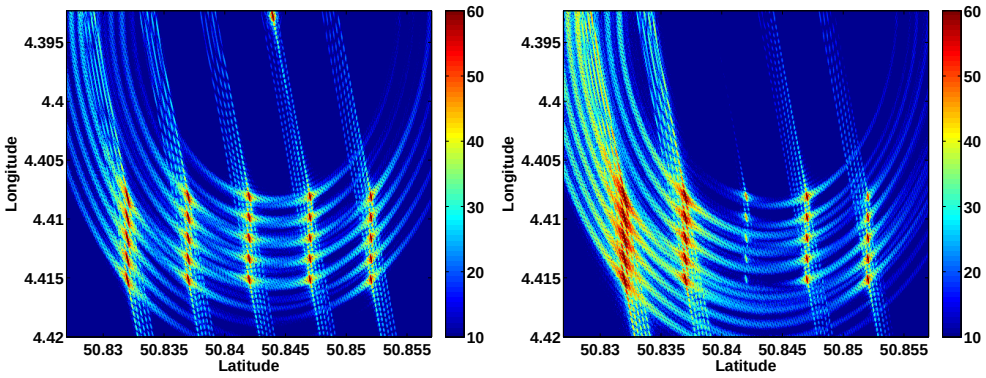

(a) (b)

Figure 4: (a) Without beamforming: the direct path signal is visible in the upper part of the image. (b) With beamforming: the direct path signal has vanished, but some scatterers have been attenuated as well.

This shadowed area can be bypassed by reorienting the ULA such as the θ_i cone is not in the desired direction of imaging.

4.2 Apodization

The second strategy to reduce these sidelobes is the method of apodization using weighting functions such as Hamming windows as described in [10]. Apodization can be performed in range or in azimuth compression or both.

First, results with ENVISAT data are used to qualitatively study the performance of the apodization in range. A satisfactory sidelobe reduction is achieved with the Hamming window as shown in Fig. 5 at the expense of a broadening of the mainlobe width and thus a

degradation of the range resolution. As a conclusion of the Hamming apodization, a point scatterer in the direction of the direct path should have an amplitude of minimum 30 dB below the direct signal and further than 30 m to be imaged. A better reduction of the sidelobes with Blackman apodization was expected. This is not the case and can be explained by the presence of noise in the real data.

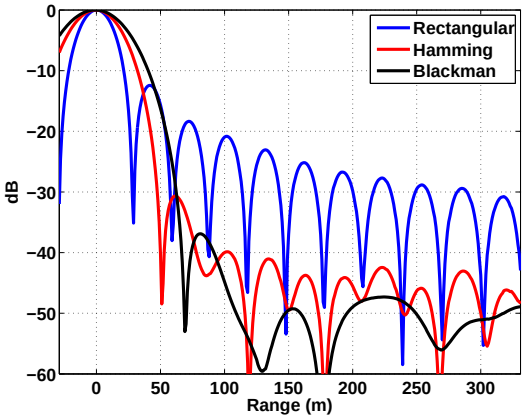

Figure 5: Effect of apodization on range sidelobes after compression of the ENVISAT transmitted signal.

Next, we consider a scenario with a point scatterer with an amplitude of -40 dB below the direct signal. Figure 6 depicts the intensity (dB) of the azimuth compressed data. The range lines are radial from the receiver while the azimuth lines are ellipses around the receiver. Figure 6 (a) illustrates the effect of the azimuth and the range sidelobes in the tangential plane at the receiver and demonstrates that point scatterers on the bistatic baseline (transmitter-receiver) will be hidden by the range sidelobes of the strong direct path signal. In Fig. 6 (b), the simulated point scatterer is also visible by using the Hamming apodization during the range compression while it was less visible without apodization (Fig. 6 (a)). If azimuth apodization is performed during the image synthesis, one can see on Fig. 6 (c) a diminution of the azimuth sidelobes of the point scatterer at the expense of a loss in azimuth resolution.

A salient observation is that the imaged area is more significantly hampered by the range sidelobes than by the azimuth sidelobes of the direct signal.

Finally, Fig. 6 (d) shows the result of spatial adaptive nullsteering where the direct signal is significantly attenuated.

5 Conclusions

This paper studies the salient impact of the strong direct signal for a non-cooperative bistatic SAR. Two strategies have been considered to mitigate its effect: spatial adaptive nullsteering and apodization of the matched filter. The first one remains the paramount method to attenuate and even suppress the direct path signal if an accurate array calibration is performed. If the attenuation of the direct signal is not sufficient, apodization can be used to complement the nullsteering method.

The results suggest that the useful imaged area (i.e. without direct signal sidelobe interference) strongly depends on the performance of both methods. Furthermore, the observation area along the bistatic baseline will never be imaged due to either the high range sidelobes of the direct path signal or the null steered in the direction of the transmitter which yields a shadowed area.

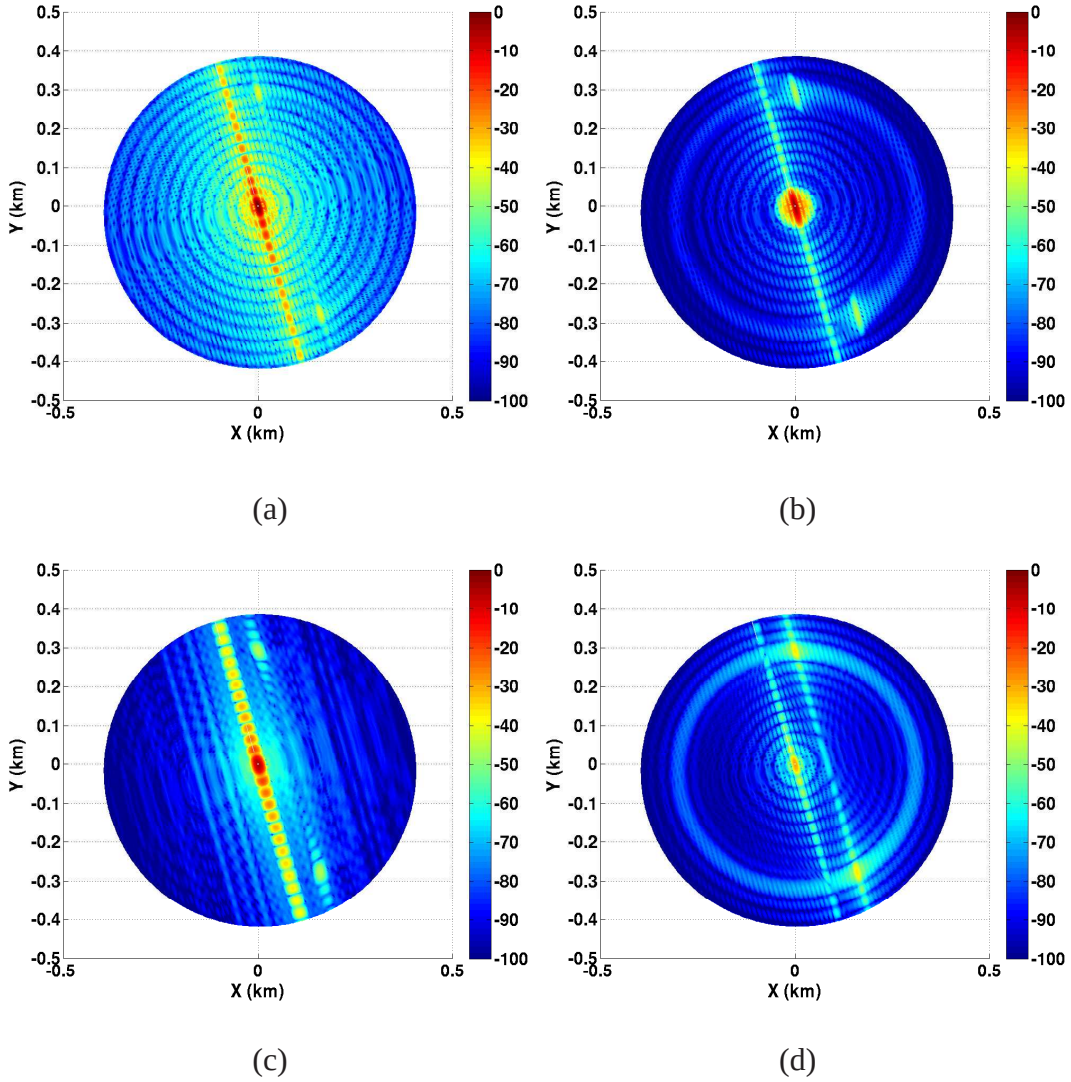

Figure 6: Azimuth compression of a signal containing a simulated target (300 m from the receiver) (a) using the strict matched filter, (b) using range sidelobe apodization (Hamming), (c) using azimuth sidelobe apodization (Hamming) and (d) after spatial adaptive nullsteering.

6 Future work

The array calibration is of utmost importance for effective spatial adaptive nullsteering. Moreover, calibration on the field could improved the performance as stated in [2].

These simulations will further be validated on real data to illustrate the performance of spatial adaptive nullsteering, the effect of shadowed area and the impact of calibration.

References

[1] M. Kubica, V. Kubica, X. Neyt, J. Raout, S. Roques, and M. Acheroy, "Optimum target detection using transmitters of opportunity," in *IEEE Radar Conference*, (Verona, NY), pp. 417–424, Apr. 2006.

[2] V. Kubica, R. Hock, E. Cristofani, and X. Neyt, "Strategies for the calibration of an array of patch antennas in passive bistatic SAR imaging," in *Proc. of the IEEE Radar conference*, (Kansas City, MI), May 2011.

[3] M. Cherniakov, "Space-surface bistatic synthetic aperture radar - prospective and problems," in *RADAR 02*, pp. 22–25, Oct. 2002.

[4] E. Cristofani, V. Kubica, and X. Neyt, "A multibeam opportunistic SAR system," in *Proc. of the IEEE Radar conference*, (Kansas City, MI), May 2011.

[5] J. Sanz-Marcos, P. Lopez-Decker, J. J. Mallorqui, A. Aguasca, and P. Prats, "SABRINA: A SAR bistatic receiver for interferometric applications," *IEEE Geoscience and Remote Sensing Letters*, vol. 4, Apr. 2007.

[6] N. J. Willis and H. D. Griffiths, *Advances in Bistatic Radar*. Raleigh, NC: SciTech Publishing, 2007.

[7] S. M. Kay, *Fundamentals of statistical signal processing — Estimation theory*. Englewood Cliffs, NJ: Prentice-Hall, 1993.

[8] J. Ward, "Space-time adaptive processing for airborne radar," Tech. Rep. 1015, MIT Lincoln Laboratory, Lexington, MA, Dec. 1994.

[9] D. G. Manolakis and J. G. Proakis, *Digital Signal Processing*. USA: Prentice Hall International, 1996.

[10] L. R. Varshney and D. Thomas, "Sidelobe reduction for matched filter range processing," in *IEEE Radar Conference*, (Huntsville, AL), pp. 446–451, May 2003.